OPEN ACCESS
IOP Publishing
Journal of Physics B: Atomic, Molecular and Optical Physics
J. Phys. B: At. Mol. Opt. Phys. **55** (2022) 184004 (14pp)
https://doi.org/10.1088/1361-6455/ac864f

Cavity QED photons for quantum information processing

Moteb M Alqahtani[1], Mark S Everitt[2] and Barry M Garraway[3,*]

[1] Department of Physics, King Khalid University, Abha, Asir, 61421, Saudi Arabia
[2] National Institute of Informatics, 2-1-2 Hitotsubashi, Chiyoda-ku, Tokyo 101-8430, Japan
[3] Department of Physics and Astronomy, University of Sussex, Falmer, Brighton, BN1 9QH, United Kingdom

E-mail: b.m.garraway@sussex.ac.uk

Received 15 April 2022, revised 22 July 2022
Accepted for publication 1 August 2022
Published 22 August 2022

Abstract

Based on a cavity QED framework, we theoretically describe a universal set of logic gates which are implemented by passing a multi-level atom initially in its ground state through a multi-mode cavity. The qubits are encoded on the cavity modes and the atom plays the role of an ancilla which will not be entangled with the final result of a gate operation. We apply the multiphoton resonance theory of Shore to develop effective two- and three-level Hamiltonians, so that the proper values for detunings, coupling coefficients, and interaction times for gate operations can be determined. This enables us to examine a faster iSWAP gate than our previous study and to examine numerically the effects of decoherence on both the iSWAP gate and our previously presented Fredkin gate which used the same multi-mode approach. We also present results that show how conditional measurements of the ancilla atom can improve gate fidelities in these cases.

Keywords: cavity QED, multi-level system, multi-photon interaction, quantum gates

(Some figures may appear in colour only in the online journal)

1. Introduction

Photonic systems are an attractive choice for quantum information processing because photons form a natural interface with optical telecommunications and existing telecoms technology. However, challenges emerge such as the generation of single photons [1–4] and enabling gates by effecting interactions between photonic qubits [5–13]. In this paper we take a slightly different approach, where we use the strong coupling of stored cavity photons to 'flying' atomic systems to produce photonic quantum gates as we introduced in reference [14]. We will extend the previous work to include analysis of a different realisation of the gate, which we call fast-iSWAP, and we examine some of the effects of decoherence this system and a previously studied Fredkin gate [14].

The workhorse of our approach uses multi-photon interactions between stored cavity photons which are mediated by an atomic system. The effect of the interaction is to shuffle photons between cavity locations. The atomic system is supposed to leave the system in the same state as it entered, having done the requisite shuffling of photons between cavity modes. In this way the ancilla atom differs from the ancilla atom in ancilla driven quantum processing [15] where measurement projections on the ancilla affect the state of the computing system. In the case studied here, a projective measurement on the atom will be a measurement on a system which has approximately disentangled from the computational modes. In fact, such a measurement can be used to improve gate fidelity.

There are many existing cavity-QED Quantum processing schemes (see for example the reviews [12, 16]), and many circuit-QED quantum processing schemes (see for example the review [17]). What is different about the set-up we study

* Author to whom any correspondence should be addressed.

here is the combination of dual-rail cavity qubits and the gate being driven by an ancilla atom that leaves (ideally) in the same state that it entered in. For a gate with two logical qubits, this means an interaction with potentially four cavity modes and two photons. The strong couplings that are, especially now, possible in cavity-QED [18] make this feasible. We try to avoid using resonant excited atomic states by being off-resonant, and this reduces spontaneous emission (at a cost of longer gate times). Cavity decay is an issue, but the dual-rail scheme ensures that photon loss is detectable as the system then leaves the computational Hilbert space. As mentioned above, a probabilistic element can be introduced by measuring the ancilla (as we will discuss further below), but for the gate in a good condition not only is the probability high, but the measurement process itself improves the gate fidelity [14].

In the following, we will use the language of photons and atoms, but in considering the experimental realisations of our multi-photon systems we can also consider microwave photons interacting with Rydberg atoms [19] or superconducting qubit systems [17, 20–22].

Because we use multi-photon processes it is very important to give careful consideration to energy level-shifts and effective couplings. For this purpose, the theoretical approach developed by Shore [23] has been invaluable to analyse two- and three-qubit gate systems by generalising it to atom-cavity systems. In this way we find locations of the resonances from the use of effective two- and three-level Hamiltonians, and from an application of this theory a set of universal gates have been devised [14, 24, 25]. Here we extend the use of Shore's method to build a faster gate and we investigate the influence of atomic and photonic relaxations on our gates.

In the following we consider some multimode, multi-Λ cavity QED systems, and their background, for quantum information processing. In section 2 we set the scene for the iSWAP gate and introduce a four-mode double-Λ system as in reference [14]. Section 3 examines the dynamics of the four mode resonance with and without intermediate resonant states; intermediate resonant states can achieve a speed-up. We also show how conditional measurements of the ancilla atom can improve gate fidelity before an examination of decoherence effects in section 4. Some three-qubit gates and single qubit rotations are examined in section 5. The paper concludes in section 6 and several appendices follow with details of the calculations of effective Hamiltonians for these multi-state, multimode systems.

2. Model two-qubit system

A simple way to realise single photonic qubits would be if the presence of a photon signifies a state $|1\rangle$ and the absence of the photon indicates the state $|0\rangle$. However, such an approach is widely recognised as being vulnerable to decoherence, which has the effect of changing qubits to $|0\rangle$. Instead, we encode our cavity qubits as dual-mode (or dual-'rail' [6, 26, 27]) cavity qubits [14]. The dual-mode qubits are formulated, for example, as shown in table 1. In this approach a qubit state is always encoded with a single excitation, as in the dual-'rail' approach, and this ensures that if a cavity decay process takes place, we have the transition $|1\rangle|0\rangle \rightarrow |0\rangle|0\rangle$, and then the result is not a valid qubit in this encoding. Physically, the difference between the two logical qubit states of table 1 is the choice of cavity mode for the location of the excitation, as indicated in figure 1.

Table 1. Dual-mode qubit coding of the scheme represented in this work.

Physical EM modes		Logical qubit
$\|1\rangle\|0\rangle$	$\mapsto$	$\|1\rangle$
$\|0\rangle\|1\rangle$	$\mapsto$	$\|0\rangle$

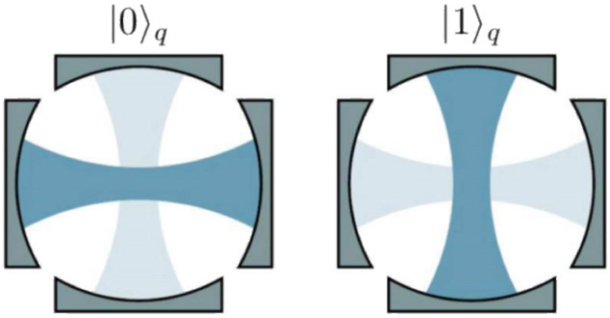

Figure 1. Schematic showing the relationship of logical qubits to cavity mode excitations (indicated as a darker colour). The case of two cavity modes is illustrated. (See table 1.)

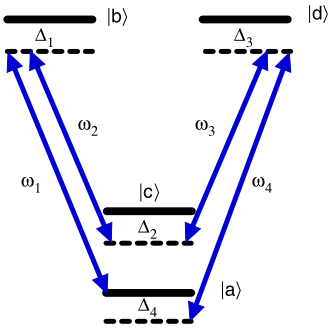

Figure 2. Scheme of two-qubit iSWAP gate, where ω_i (with $i = 1, 2, 3, 4$) are modes of the four-mode high Q cavity, and $|a\rangle$, $|b\rangle$, $|c\rangle$, and $|d\rangle$ are four energy levels of the atom.

A consequence of using the dual-mode approach is that in order to have a two-qubit gate we need to have an interaction of an atom with *four* cavity modes. As in reference [14] we will achieve this by having a sequence of off-resonant interactions with a multilevel atom (figure 2). In addition, the atom will be an ancilla which will not be entangled with the final result of a gate operation. The aim of the off-resonant interactions is to reduce spontaneous emission from the ancilla atom. In order that we do not extract 'information' from the system via the ancilla atom it is important for the sequence of atomic transitions to start and end on the same atomic state $|a\rangle$ (see figure 2). Multiphoton resonance will also require the determination of a finite final detuning, Δ_4 to ensure resonance. While Δ_4 is small, it has to have level shifts taken into account because the resonance is narrow.

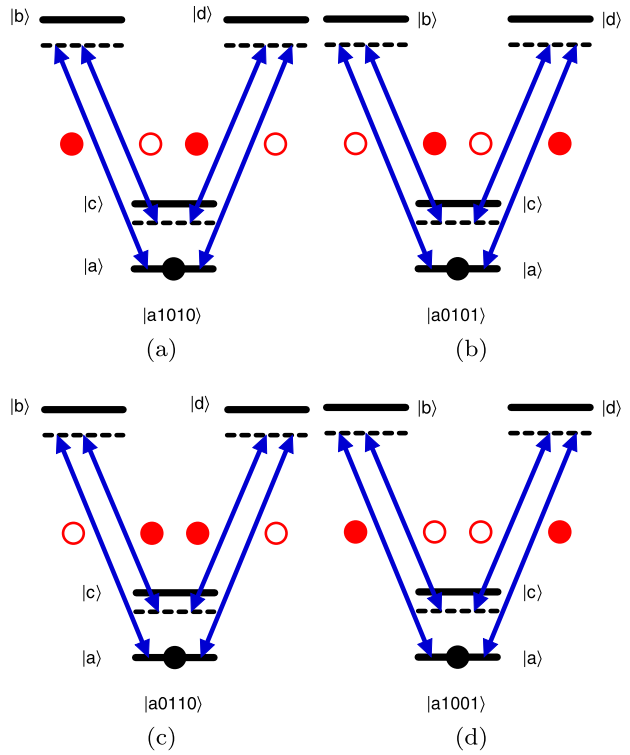

Figure 3. The four key initial states of the two-qubit (four mode) system with possible interactions. Empty red circles represent empty cavity modes and filled red circles represent cavity modes with a single excitation. The filled black circles indicate where the atomic population is located in this simplified analysis of the gate process. Starting from atomic state $|a\rangle$ we can see that (a) and (b) can progress, but (c) and (d) are blocked.

The full Hamiltonian of the four-level system is then (see for example [28, 29]):

$$\hat{H} = \sum_{i=a,b,c,d} \omega_i\ \hat{\sigma}_{ii} + \sum_{j=1}^{4} \omega_j\ \hat{a}_j^{\dagger}\hat{a}_j + \Big[g_1^{ab}\ \hat{a}_1\ \hat{\sigma}^{ba} + g_2^{bc}\ \hat{\sigma}^{cb}\ \hat{a}_2^{\dagger} + g_3^{cd}\hat{a}_3\ \hat{\sigma}^{dc} + g_4^{da}\ \hat{\sigma}^{ad}\ \hat{a}_4^{\dagger} + \text{h.c.}\Big], \quad (1)$$

where $g_k (k = 1, 2, 3, 4)$ represent the coupling strengths, and $\hat{a}_j$ is the photon annihilation operator for the cavity mode. The first two terms in the Hamiltonian $\hat{H}$ represent the non-coupling Hamiltonians, and the remaining terms describe the atom-field interaction Hamiltonian. The four key initial states of the system and their mappings to logical qubits can be summarised as

$$\begin{aligned} &\text{physical} && \text{logical} \\ &|a,\ 0110\rangle \mapsto |a,\ 00\rangle \\ &|a,\ 0101\rangle \mapsto |a,\ 01\rangle \\ &|a,\ 1010\rangle \mapsto |a,\ 10\rangle \\ &|a,\ 1001\rangle \mapsto |a,\ 11\rangle. \end{aligned} \quad (2)$$

All possible interactions and the four key initial states of the system are represented in figure 3 where we do not include configurations which cannot be represented with logical qubits. In the case of the initial state $|a,\ 1010\rangle$, the system (atom + field) is governed by the Hamiltonian $\hat{H}'$ which can be expressed, in the matrix representation and with $|a,\ 1010\rangle$ to be the zero-point energy, as

$$H' = \begin{pmatrix} 0 & g_1^{ab} & 0 & 0 & 0 \\ g_1^{ab} & \Delta_1 & g_2^{bc} & 0 & 0 \\ 0 & g_2^{bc} & \Delta_2 & g_3^{cd} & 0 \\ 0 & 0 & g_3^{cd} & \Delta_3 & g_4^{da} \\ 0 & 0 & 0 & g_4^{da} & \Delta_4 \end{pmatrix}, \quad (3)$$

in the basis states $\{|a\ 1010\rangle, |b\ 0010\rangle |c\ 0110\rangle |d\ 0100\rangle |a\ 0101\rangle\}$.

Starting with different logical qubits, i.e. different arrangements of the excited modes, the multiphoton process is blocked in the case of $|a\ 0110\rangle$. In figure 3(c) there is no cavity photon available in the first and last modes to raise the atomic state from $|a\rangle$. When the initial state is $|a\ 1001\rangle$ (figure 3(d)), on the other hand, the evolution of the system is governed by the Hamiltonian $\hat{H}''$ given as the matrix

$$H'' = \begin{pmatrix} \Delta_2 & g_2^{bc} & 0 & 0 & 0 \\ g_2^{bc} & \Delta_1 & g_1^{ab} & 0 & 0 \\ 0 & g_1^{ab} & 0 & g_4^{da} & 0 \\ 0 & 0 & g_4^{da} & (\Delta_3 - \Delta_4) & g_3^{cd} \\ 0 & 0 & 0 & g_3^{cd} & (\Delta_2 - \Delta_4) \end{pmatrix}, \quad (4)$$

acting in the basis states $\{|c\ 0101\rangle, |b\ 0001\rangle, |a\ 1001\rangle |d\ 1000\rangle |c\ 1010\rangle\}$.

3. Two-qubit four-mode gate

In this section we will use the model of the previous section 2 and reference [14] to produce an iSWAP gate in two different ways by determining an approximate Hamiltonian involving either two states (as in reference [14]) in section 3.1, or three states (in section 3.2). Because the time evolution of the iSWAP gate exhibited in the following section 3.1 is slow, we can achieve a speed-up by allowing some of the intermediate states in figure 2 to become resonant: this is the motive for moving to an effective three-level system. A similar approach was taken to speed up the three-qubit Fredkin gate in reference [14] (also discussed further in section 5. There are a wide range of possibilities when it comes to choosing an intermediate state in the two-qubit four-mode system. Our choice of system needs to be informed by which configurations can keep the qubit state $|a11\rangle$ in its initial state at the appropriate interaction time.

To easily identify the different model systems we will introduce a binary type notation to indicate which levels in the sequence of states are to be resonant, and which are not. Thus the model (10001) has only two resonant states in the chain, the first and last ones, and will be treated in section 3.1 below. If we took a fully resonant model, where every transition is resonant, the model would be identified as model (11111). However, being resonant, this configuration is extremely vulnerable to decoherence. Instead, in section 3.2 we will focus on model

(11001), as one of the cases with three resonant levels which is faster than model (10001) and less prone to decoherence than model (11111).

3.1. An effective two-level system for the iSWAP gate

Here we consider model (10001) which realises an effective two-level system to shuffle the cavity excitations. We presented this model in reference [14] and include it here for direct comparison in the next section 3.2. For the initial state $|a\ 1010\rangle$, the effective wave-function of the system can be expressed as:

$$|\Psi(t)\rangle = c_1|a\ 1010\rangle + c_2|b\ 0010\rangle + c_3|c\ 0110\rangle + c_4|d\ 0100\rangle + c_5|a\ 0101\rangle, \tag{5}$$

which is a superposition of the key states used for single photon swapping.

In appendix A we present the general theory, adapted from Shore [23], for extracting an effective Hamiltonian for the system by utilizing the theory of multiphoton resonance for the adiabatic elimination of the unwanted (off-resonant) levels as shown in figure 2. The detailed case of the effective two-level Hamiltonian is presented in appendix B1 where we use the basis of equation (5) to develop an effective two-level Hamiltonian which takes the form

$$H_{\text{eff}} = \begin{bmatrix} 0 & g_{\text{eff}} \\ g_{\text{eff}} & \Delta_{\text{eff}} \end{bmatrix}, \tag{6}$$

where ($g \ll \Delta$) is required (see appendix B1). The effective coupling is found to be

$$g_{\text{eff}} \approx -\frac{g_1^{ab} g_2^{bc} g_3^{cd} g_4^{da}}{\Delta_1 \Delta_2 \Delta_3}, \tag{7}$$

and the effective detuning of the two-level system is

$$\Delta_{\text{eff}} \approx \Delta_4 + \frac{(g_1^{ab})^2}{\Delta_1} - \frac{(g_4^{da})^2}{\Delta_3}. \tag{8}$$

The time evolution of this system is given by the following equations for the logical states,

$$\begin{aligned} |a,10\rangle &\mapsto \cos(g_{\text{eff}}t)|a,10\rangle - i\ \sin(g_{\text{eff}}t)|a,01\rangle \\ |a,01\rangle &\mapsto \cos(g_{\text{eff}}t)|a,01\rangle - i\ \sin(g_{\text{eff}}t)|a,10\rangle. \end{aligned} \tag{9}$$

This two-level system undergoes a swapping of the states $|a\ 1010\rangle$ and $|a\ 0101\rangle$ when the resonance condition is achieved by setting Δ_{eff} to zero in equation (8). This is illustrated in figure 4 where excellent agreement between an exact numerical calculation and the analytic treatment of equation (9) is presented. Because of the finite value of Δ chosen in figure 4, a fine high frequency oscillation can be seen. For larger detuning this oscillation becomes smaller as the two-level approximation is realised more accurately.

The effective Hamiltonian (6) only connects the states $|a\ 1010\rangle$ and $|a\ 0101\rangle$; the state $|a\ 1001\rangle$ is effectively governed instead by the full Hamiltonian (4), and the other logical state of the system, $|00\rangle$, is unchanged. Considering the parameters in figure 4 and at the special time $g_{\text{eff}}t = \pi/2$, we obtain the following outputs for the basic inputs (see figure 5):

Input	Output
$\|00\rangle$	$\|00\rangle$
$\|01\rangle$	$i\|10\rangle$
$\|10\rangle$	$i\|01\rangle$
$\|11\rangle$	$\|11\rangle$

(10)

This realises an iSWAP gate and we can represent the above mappings as the table (note that a global phase can be produced as we see below)

$$\text{iSWAP} \equiv \begin{bmatrix} 1 & & & \\ & 0 & i & \\ & i & 0 & \\ & & & 1 \end{bmatrix}. \tag{11}$$

The iSWAP gate is a universal gate when combined with single qubit rotations. For example it can be directly related to the CNOT gate (also a universal gate) by means of a quantum circuit as shown in reference [30]. It has been shown that the iSWAP gate can be very useful for applications in quantum information processing and quantum computing, for example, the replacement of the standard CNOT gate by the iSWAP gate provides a more efficient, simpler, and faster way of generating cluster states [31], which play a crucial role in the so-called one-way quantum computation approach [32, 33].

3.2. An effective three-level system for the iSWAP gate

In order to increase the operational speed of the gate presented in the previous section (and reference [14]), we now use the model (11001), where we set $|b\ 0010\rangle$ to be resonant. We apply the adiabatic elimination theory (as shown in appendix B2) to obtain an effective three-level system in the reduced space of states $\{|a\ 1010\rangle, |b\ 0010\rangle, |a\ 0101\rangle\}$. The effective couplings are found to be

$$g_{\text{eff}}^{(1)} = g_1^{ab}, \qquad g_{\text{eff}}^{(2)} \approx \frac{g_2^{bc} g_3^{cd} g_4^{da}}{\Delta_2 \Delta_3}, \tag{12}$$

and the effective detunings

$$\begin{aligned} \Delta_{\text{eff}}^{(1)} &\approx \Delta_1 - \frac{(g_2^{bc})^2}{\Delta_2}, \\ \Delta_{\text{eff}}^{(2)} &\approx \Delta_4 - \frac{(g_4^{da})^2}{\Delta_3}. \end{aligned} \tag{13}$$

The resulting Hamiltonian takes the form

$$H_{\text{eff}} = \begin{bmatrix} 0 & g_{\text{eff}}^{(1)} & 0 \\ g_{\text{eff}}^{(1)} & \Delta_{\text{eff}}^{(1)} & g_{\text{eff}}^{(2)} \\ 0 & g_{\text{eff}}^{(2)} & \Delta_{\text{eff}}^{(2)} \end{bmatrix}. \tag{14}$$

The time evolution of this gate is shown in figure 6(a) and it is immediately apparent that the population swapping happens much faster than the evolution seen in figure 4 for model

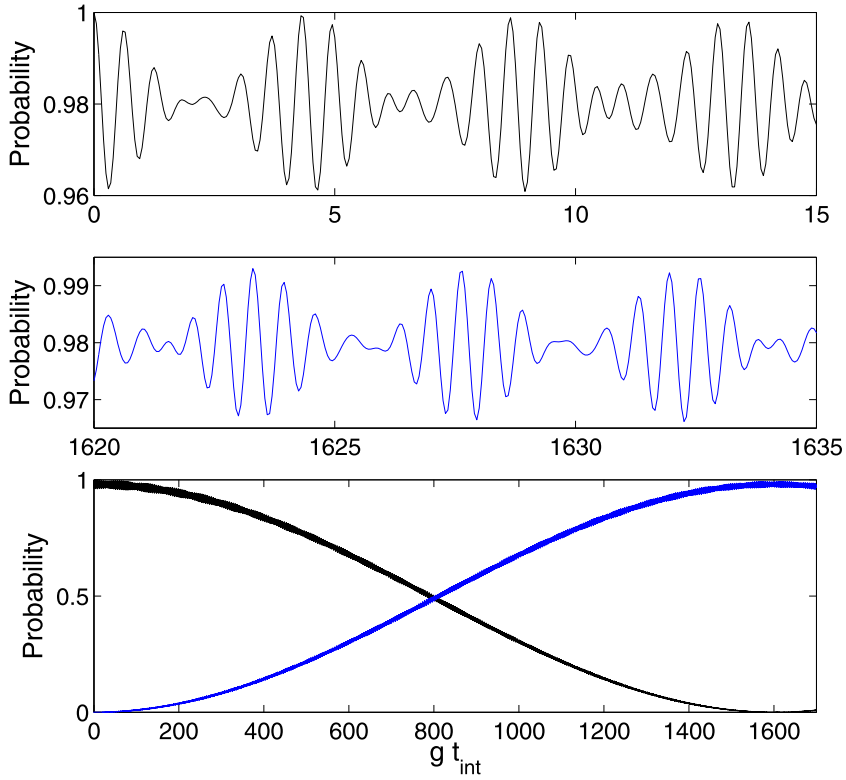

Figure 4. Population swapping in the model (10001). All couplings g_j ($j = 1, 2, 3, 4$) are set to g, and the detunings Δ_i with $i = 1, 2, 3$ are set to Δ. The value of Δ_4 is determined by Equation (8). The two upper figures show zooms for the population.

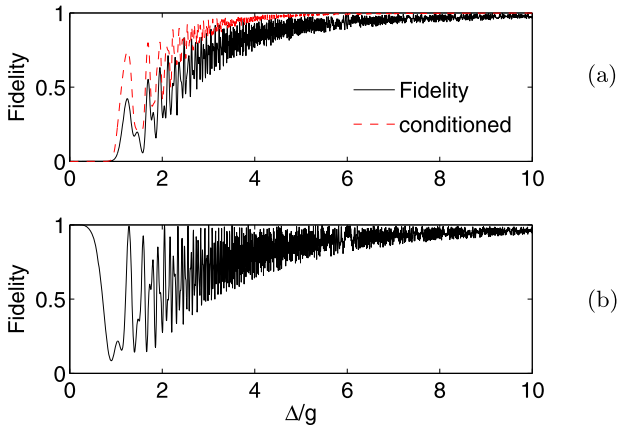

Figure 5. (a) The fidelity (black line) of swapping between the logical states $|a\ 10\rangle$ and $|a\ 01\rangle$ in the model (10001). The red-dashed line shows the conditional fidelity. (b) The fidelity of keeping the system initially in the logical state $|a\ 11\rangle$. Parameters of the detunings Δ and the coupling strengths g are defined in figure 4.

(10001). From the Hamiltonian (14) the time evolution of the swapping follows the equations (for the initial state $|a, 1010\rangle$)

$$|a,10\rangle \to \left[\frac{(g_{\rm eff}^{(1)})^2}{\overline{g}^2} + \frac{(g_{\rm eff}^{(2)})^2}{\overline{g}^2}\cos(\overline{g}t)\right]|a,10\rangle - i\frac{g_{\rm eff}^{(1)}}{\overline{g}}\sin(\overline{g}t)|\Phi\rangle + \frac{g_{\rm eff}^{(1)}g_{\rm eff}^{(2)}}{\overline{g}^2}[\cos(\overline{g}t)-1]e^{i\zeta t}|a,01\rangle, \quad (15)$$

where $\overline{g} = \sqrt{(g_{\rm eff}^{(1)})^2 + (g_{\rm eff}^{(2)})^2}$ and $|\Phi\rangle \equiv |b\ 0010\rangle$.

By setting $\overline{g}t = \pi$ and $\zeta t = \pi$ (with $g_{\rm eff}^{(1)}t = g_{\rm eff}^{(2)}t = \pi/\sqrt{2}$), the transformation $|a\ 1010\rangle \to |a\ 0101\rangle$ and $|a\ 0101\rangle \to |a\ 1010\rangle$ can take place. The additional phase factor ζt in equation (15) can be engineered with, for example, the single-qubit gate in section 5.4.

In figure 6(a), we plot the population of the states corresponding to those in equation (15). By substituting the parameters of the coupling constants and detunings in the model (11001) into the Hamiltonian (4) which describes the time evolution of the initial state $|a\ 1001\rangle$, it is noticeable that this state can be sufficiently forced to stay in its initial state, as demonstrated by the red-dashed line in figure 6(b). We then obtain table 11 and the iSWAP gate is realized in a way that is faster than the version presented in reference [14].

3.3. Enhancement of two-qubit gate conditional on measurements

In the scheme we have developed so far the atom plays the role of an ancilla which simply 'enables' the shuffling of energy between cavity modes. However, if the proposed gate is slightly imperfect there will be a small admixture of other atomic states. Bearing in mind that the ancilla atom is supposed to remain in the same state at the end of the shuffling, the role of a conditional measurement on the ancilla is to improve the quality of the final state (i.e. to improve the fidelity). (A similar technique was applied to the Fredkin gate in reference [14].)

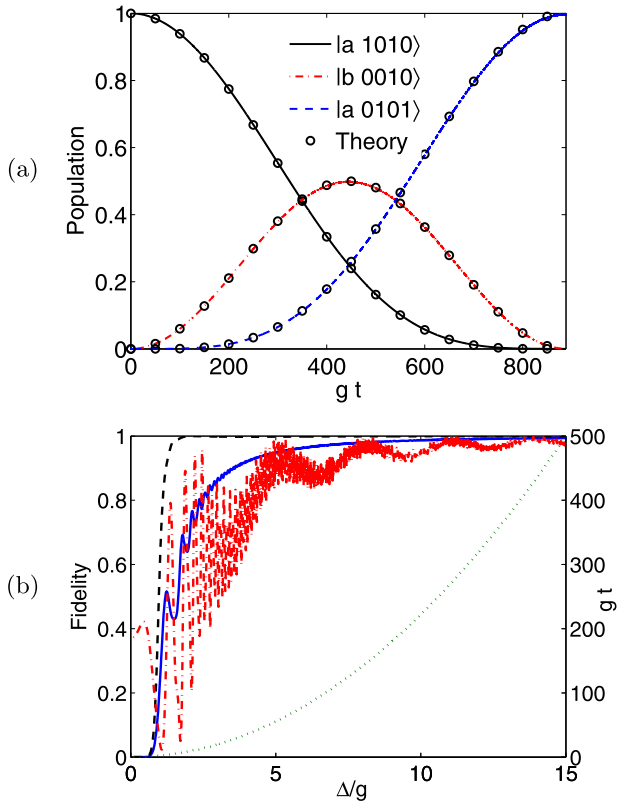

Figure 6. Three-level fast-iSWAP behaviour with the states $|c\rangle$ and $|d\rangle$ chosen to be highly-detuned (see figure 2). Parameters: the coupling constants $g_{2,3,4}$ are all set to g, and the detunings $\Delta_{2,3}$ are set to Δ. (a) The probability of the states $|a\ 1010\rangle$ (solid black line), $|b\ 0010\rangle$ (red chained line), and $|a\ 0101\rangle$ (blue dashed line) as a function of time with $\Delta = 20g$. The circles are the theory prediction of equation (15) and fit very well. (b) The numerically calculated fidelity of mapping logical $|a\ 10\rangle$ to $|a\ 01\rangle$ (blue-solid line), and the fidelity of logical $|a\ 11\rangle$ remaining in its initial state (red dotted-dashed line), both shown as a function of detuning Δ. The black-dashed line represents the conditioned state fidelity (section 3.3). The green-dotted line is the interaction time gt_{int} (on the right axis) which varies with Δ and is used to determine the time at which the fidelities are calculated.

For example, let us suppose the state of the system is

$$|\Psi(t)\rangle = c_1|a\ 1010\rangle + c'|c\ 0110\rangle + c_2|a\ 0101\rangle + \cdots \quad (16)$$

Then if the atom exits the system in state $|a\rangle$ we must project the state (16) onto the atomic state $|a\rangle$ to obtain the conditioned result

$$|\Psi(t)\rangle' \rightarrow \frac{c_1}{\sqrt{|c_1|^2+|c_2|^2}}|a\ 1010\rangle + \frac{c_2}{\sqrt{|c_1|^2+|c_2|^2}}|a\ 0101\rangle. \quad (17)$$

Because of the renormalisation that takes place this conditionally enhances a desired result (such as $|a\ 0101\rangle$).

To a limited extent this makes the scheme probabilistic. However, the probability of success in such a measurement is expected to be high and the intent is that this measurement process simply enhances the result and cleans up the wavefunction. The red-dashed line in figure 5(a) and black-dashed line in figure 6(b) show significant improvement of fidelity in the models (10001) and (11001) by means of this approach.

4. The effect of decoherence

Decoherence is a significant concern in quantum information processing systems. For that reason we are motivated to examine the sensitivity to decoherence, which was not included in our previous paper [14]. The time evolution our system (1) in the presence of decoherence can be governed by Liouville's equation

$$\frac{\partial}{\partial t}\,\hat{\rho} = -i[\hat{H}',\ \hat{\rho}] + \mathcal{L}\,\hat{\rho}, \quad (18)$$

where $\hat{\rho}$ is the density operator of the atom-field system and the so-called Liouvillian operator $\mathcal{L}\hat{\rho}$ describes the dissipative mechanisms in the system. The general Lindblad form of the Liouvillian operator $\mathcal{L}\hat{\rho}$ can be expressed as [34]

$$\mathcal{L}\,\hat{\rho} = \sum_i \frac{\eta_i}{2}\left([\hat{L}_i\,\hat{\rho},\ L_i^\dagger] + [\hat{L}_i,\ \hat{\rho}\,L_i^\dagger]\right), \quad (19)$$

where η_i represents the loss of population and coherence through decay channel i. which can be due to either spontaneous emission at rate Γ, or to the cavity field decay at a rate κ. The operators $\hat{L}$ and $\hat{L}^\dagger$ are the corresponding system operators. More explicitly, in the presence of the atomic decay $\hat{L}$ and $\hat{L}^\dagger$ can be replaced by the atomic operators $\hat{\sigma}_-$ and $\hat{\sigma}_+$ of the relevant atomic state, and in the case of the cavity decay they are represented by the field operators $\hat{a}$ and $\hat{a}^\dagger$ for the relevant cavity mode. Variation in the fidelity of the iSWAP gate in the existence of atomic and photonic decays can be therefore numerically calculated (see figure 7).

The numerical results provided by the general master equation above can be understood by deriving analytical solutions. To this end, we now apply the theoretical treatment known as the wave function method [35–41], or master equation unravelling, on the system (5). We rewrite the previous Liouville equation in equation (18) as

$$\frac{\partial}{\partial t}\,\hat{\rho} = -i(\hat{H}'_{\text{eff}}\,\hat{\rho} - \hat{\rho}\,\hat{H}'^{\dagger}_{\text{eff}}) + J\,\hat{\rho}, \quad (20)$$

where $\hat{H}'_{\text{eff}} = \hat{H}' - \frac{i}{2}\sum_i \eta_i\,\hat{L}_i^\dagger\hat{L}_i$, (with $\hat{H}'$ being the original Hamiltonian of the system in the absence of any decay), and $J\,\hat{\rho} = \sum_i \eta_i\,\hat{L}_i\,\hat{\rho}\,\hat{L}_i^\dagger$. Now, to investigate the influence of the atomic and photonic relaxations we simply build the non-Hermitian Hamiltonian $\hat{H}'_{\text{eff}}$, reapply the Shore's method for producing the effective two- and three-level Hamiltonians, and then propagate the wave function $|\Psi(t)\rangle$ in equation (5) with the Schrödinger equation using these Hamiltonians. This procedure is valid since the atomic and photonic decays in our systems result in an irreversible loss of population, and therefore no photon is detected [36, 37, 42]. In this work, it is observed that the system in each input state, in both the iSWAP and the Fredkin gates, is not closed and decay channels in all these systems result in an irreversible loss of population. Part of the reason for this is the use of the dual-'rail' qubit representation of equation (2) where qubit decay results in a state which is out of the space of the logical qubits.

Given the initial states to be either $|a\ 1010\rangle$ or $|a\ 0101\rangle$ and starting with the model (10001), the time evolution of the state

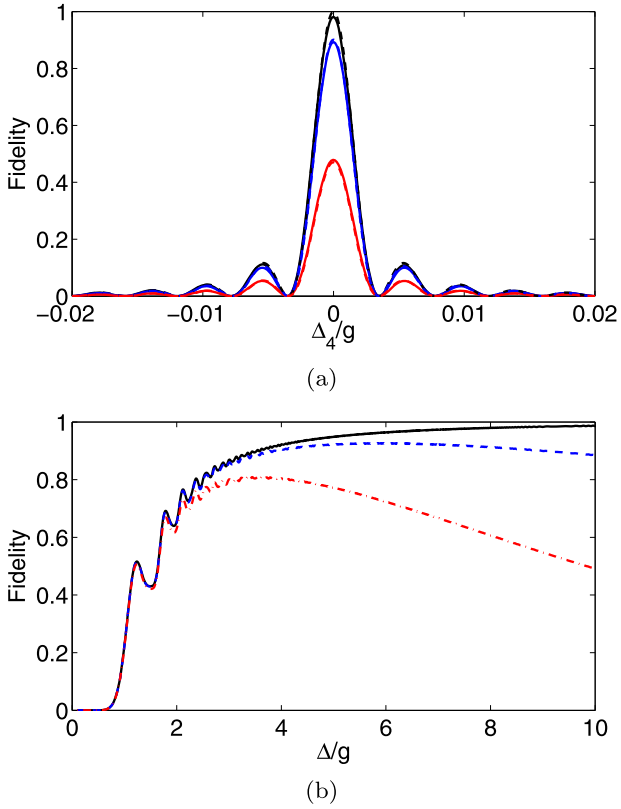

Figure 7. The influence of the dissipative mechanisms on the qubit state $|a\ 10\rangle$ or $|a\ 01\rangle$ in the models (10001) and (11001) after a gate operation. The three curves in these two plots represent a resonant fidelity of $F = (1, 0.9, 0.5)F_0$ where F_0 represents the fidelity of the system at the resonance point in the absence of any decay. (a) In the model (10001), the three curves corresponding to the values of photonic decays $\kappa \sim (0, 0.033, 0.24)g_{\rm eff}$ with $\Delta = 10g$. The solutions by theory (dashed lines) and simulation (solid lines) are highly matched for moderate κ and are shown as a function of the final detuning Δ_4. (b) In the model (11001) the three curves correspond photonic decay rates $\kappa \sim (0, 0.025, 0.185)\bar{g}/\sqrt{2}$ when no atomic decay rate is considered.

$|a\ 0101\rangle$ in the strong coupling regime is

$$c_{a01}(t) = -i\frac{g_{\rm eff}}{\tilde{g}}\, e^{-\kappa t}\, \sin(\tilde{g}t)e^{-i\Delta_{\rm eff}t/2}, \qquad (21)$$

where $\tilde{g} = \sqrt{g_{\rm eff}^2 + (\Delta_{\rm eff}/2)^2}$ (with $g_{\rm eff}$ and $\Delta_{\rm eff}$ are defined in equations (7) and (8). The norm of the system shows that it decays with the rate (2κ). Figure 7(a) demonstrates the fidelity for different values of κ. As we have mentioned before, the iSWAP gate formed from the model (10001) in section 3.1 is relatively slow and, therefore, it is very sensitive to photonic decay rates.

In the case of the model (11001), the eigenvalues for the resultant effective Hamiltonian can be determined, under the condition $2\bar{g} \geqslant (\kappa - 2\Gamma)$ and with vanishing effective detunings, as

$$\lambda_1 = -\kappa, \qquad \lambda_{2,3} = -\left(\frac{3\kappa + 2\Gamma}{4}\right) \pm i\lambda, \qquad (22)$$

where $\lambda = \{\bar{g}^2 - \frac{1}{4}(\kappa - 2\Gamma)^2\}^{1/2}$, $\bar{g} = \sqrt{(g_{\rm eff}^{(1)})^2 + (g_{\rm eff}^{(2)})^2}$, and $g_{\rm eff}^{(1)}$ and $g_{\rm eff}^{(2)}$ are the effective coupling constants in equation (12). The corresponding eigenvectors can be found and then the time evolution of the logical state $|a\ 01\rangle$ can be expressed as

$$c_{a01}(t) = \frac{g_{\rm eff}^{(1)} g_{\rm eff}^{(2)}}{\bar{g}^2}\, \exp(-\kappa t) \times \left\{-1 + \left[\cos(\lambda t) - \left(\frac{\kappa - 2\Gamma}{4\lambda}\right)\sin(\lambda t)\right] \times \exp\left(\frac{\kappa - 2\Gamma}{4}t\right)\right\}, \qquad (23)$$

for the initial condition that the system is completely set in the initial state $|a\ 1010\rangle$ at $t = 0$, i.e. $c_{a10}(0) = 1$.

In figure 7(b) we consider the model (11001) and measure the fidelity at different values of κ. Figure 7 shows that the impact of cavity field relaxation is less in the model (11001) when compared to the model (10001), and this is because of the improvement in the qubit states speed.

We now discuss the feasibility of implementing the iSWAP gate above within recent cavity QED techniques. Considering the microwave cavity-QED experiment in [19], highly excited Rydberg atoms (typically ^{85}Rb) with a radiative time $\tau_{\rm rad} \sim$ 30 ms have been used to interact with a superconducting cavity with $Q \mapsto 4 \times 10^{10}$. The photon lifetime inside the cavity is in order $\tau_{\rm ph} \sim 130$ ms, and the coupling strength is around $g/2\pi \sim 50$ kHz. By setting $\Delta = 10$ g, this corresponds to cavity-atom interaction time $t_{\rm int} \mapsto 5$ ms in the configuration (10001), and $t_{\rm int} \mapsto \frac{1}{\sqrt{2}}$ ms in the configurations (11001). The quantity $\tau_{\rm ph}/t_{\rm int}$ shows that the last configuration is much better for QIP applications with the present cavity QED techniques.

5. Three qubit gates and rotations

In the next sections 5.1 and 5.2 we present an overview, based on reference [14], of a three qubit gate, using the methodology of appendix A. The gate we focus on is the fast Fredkin gate where, in section 5.3, we extend the study of its behaviour to cases including decoherence. The Fredkin gate is another entangling gate, but we note that to have a universal set of gate operations it is necessary to have single qubit rotations (or single qubit gates) which are discussed in section 5.4. Full details of the adiabatic eliminations are given in appendices C and D.

5.1. Three qubit gate

The three qubit scheme of figure 8 contains dual-mode qubits with a repeated mode at ω_1. The partner mode for ω_1 is not shown as it is unaffected by the logic process. The remaining pairs are $\omega_{2,3}$ and $\omega_{5,6}$, (a mode with the label ω_4 is omitted in the following analysis to avoid confusion). The consequence of the repeated mode 1 is that the chain only completes if mode 1 is present (in which case the excitation is absorbed and then re-emitted) and if modes 3 and 5 have excitations present (which

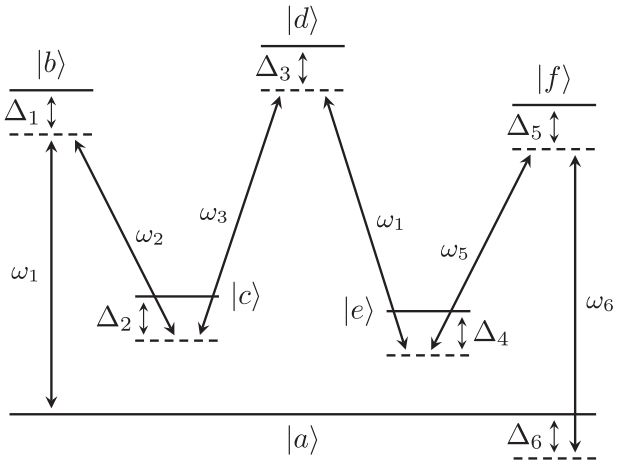

Figure 8. Energy level scheme for a Fredkin gate. Note the repeated mode ω_1. Operation requires at least $\Delta_6 \sim 0$.

implies necessary empty modes 2 and 6 in the dual-mode qubit basis). The result of all this is that the qubit 1 acts as a control qubit which swaps the qubits present in logical qubits 2 and 3: i.e. we have the logic needed for a Fredkin gate [43]. In a Fredkin gate we aim for logical qubits to be mapped as follows:

Input	Output
$\|000\rangle$	$\|000\rangle$
$\|001\rangle$	$\|001\rangle$
$\|010\rangle$	$\|010\rangle$
$\|011\rangle$	$\|011\rangle$
$\|100\rangle$	$\|100\rangle$
$\|110\rangle$	$\|101\rangle$
$\|101\rangle$	$\|110\rangle$
$\|111\rangle$	$\|111\rangle$

(24)

The Fredkin gate is a universal gate owning important properties which set up the general principles of logic gates and circuits in both classical and quantum computing [43]. This gate swaps the second and the third qubits if the first qubit is $|1\rangle$, otherwise, all qubits remain unchanged. Two examples of quantum circuits generating this gate can be considered. Firstly, it is observable that the Fredkin gate is nothing but the controlled SWAP gate [44]. Secondly, since the SWAP gate is equivalent to three CNOT gates, we can see that the Fredkin gate is a combination of the Toffoli gate together with two CNOT gates [45].

5.2. Two- and three-level configurations

For a de-excited atom interacting with multimode cavities, the realisation of the Fredkin gate at the interaction time $gt_{\rm int}$ can be achieved when the transformation $|a\ 101\rangle \leftrightarrow |a\ 110\rangle$ is made and the remaining logical qubits are in their initial states. Once again, Shore's method provides a useful tool to find out several configurations that are capable of swapping the states $|a\ 101\rangle$ and $|a\ 110\rangle$. However, to meet the truth table of the Fredkin gate, and since there is a presence of a repeated mode 1 in addition to certain over-shot states (see appendix C) it is noticed that the only possible configurations realising the gate are the models (1000001) and (1001001). In the model (1000001) we set all states other than the states $|a\ 101\rangle$ and $|a\ 110\rangle$ to be off-resonant, and in the model (1001001) a further atomic state $|d\rangle$ is allowed to be resonant. The full details of the analysis of the former model (1000001) are not presented here, it can be found in reference [14] where we also show that an excellent speed-up is obtained by choosing an intermediate resonant energy level, i.e. the model (1001001). In this case the effective Hamiltonian reduces to a three-level system again, where (see appendix C) the effective coupling constants are

$$g_{\rm eff}^{(1)} = \frac{g_1^{ab} g_2^{bc} g_3^{cd}}{\Delta_1 \Delta_2}, \qquad g_{\rm eff}^{(2)} = \frac{g_1^{de} g_5^{ef} g_6^{fa}}{\Delta_4 \Delta_5}, \tag{25}$$

and the effective detunings are

$$\Delta_1^{\rm eff} \approx \Delta_3 + \frac{\left(g_1^{ab}\right)^2}{\Delta_1} - \frac{\left(g_3^{cd}\right)^2}{\Delta_2} - \frac{\left(g_1^{de}\right)^2}{\Delta_4},$$
$$\Delta_2^{\rm eff} \approx \Delta_6 - \frac{\left(g_6^{af}\right)^2}{\Delta_5}. \tag{26}$$

Given the initial state to be either the logical $|a\ 101\rangle$ or $|a\ 110\rangle$, the sequence of effective Rabi frequencies and the evolution equation (15) can be reused to describe the swapping of qubit states $|a\ 10\rangle$ and $|a\ 01\rangle$. A high fidelity result can be obtained for sufficiently large detunings. Figure 9(a) shows how this increases, and also how the use of measurement of the ancilla atom (as in section 3.3) strongly improves the result for the quite low value of $\Delta/g \gtrsim 3$. The same figure shows the interaction time, which is fairly high for large Δ ($gt \sim 500$ for $\Delta = 15g$) but reduces substantially near $\Delta = 5g$. The fidelity for the qubit state $|a\ 100\rangle$ to remain in its initial state at the same interaction times as above has been illustrated in figure 9(b). Here we see, firstly, that the fidelity improves as Δ increases. Also, we observe a 'banding' that reduces as Δ increases. This has its origin in an adiabatic breakdown of the approximation of appendix A. As Δ increases, the adiabaticity improves, and the 'band' of oscillation decreases in width. For other qubit states, large detunings for all atomic levels except $|a\rangle$ and $|d\rangle$ ensure an efficient confinement of the populations in the desired states so that the three-qubit Fredkin gate is realised.

5.3. Decoherence in the fast Fredkin gate

Considering the parameters of the coupling constants and the detunings in the model (1001001) given by equations (25) and (26), we can use the master equation (18) to address the influence of atomic and photonic relaxations on the Fredkin gate. We can also use the non-Hermitian Hamiltonian $\hat{H}'_{\rm eff} = \hat{H}' - \frac{i}{2}\sum_i \eta_i\ \hat{L}_i^\dagger\ \hat{L}_i$ to find analytic solutions for the evolution of the input states in the Fredkin gate as these systems are not closed and the loss of population in these systems are irreversible (see the arguments of section 4). For example, for the three-level system, or fast Fredkin gate, described above the damping due to atomic and photonic decays can be studied as follows. Under the strong coupling regime, the eigenvalues of the damped three-level behaviour (1001001) can be given

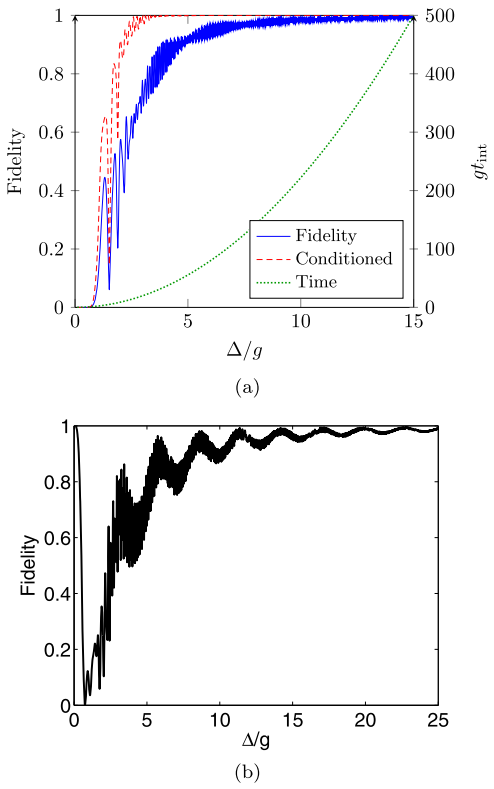

Figure 9. Fidelity for the fast Fredkin gate shown as a function of the detuning Δ where we again take $\Delta_j \to \Delta$ for $j = 1, 2, 4, 5$ with $\Delta_3 = 0$ and $\Delta_6 \sim 0$ (given by equation (26) set to zero). The initial state is (a) $|a\,101\rangle$, (b) $|a\,100\rangle$. For the couplings we take $g_j \to g$. The dashed line in (a) shows the interaction time $\bar{g}t_{\rm int} = \pi$ as found from the three-state model section 3.2.

as

$$\lambda_1 = -3\kappa/2, \quad \lambda_{2,3} = -\left(\frac{5\kappa + 2\Gamma}{4}\right) \pm i\lambda, \tag{27}$$

where $\lambda = \left(\bar{g}^2 - \frac{1}{4}(\kappa - 2\Gamma)^2\right)^{1/2}$, $\bar{g} = \sqrt{(g_{\rm eff}^{(1)})^2 + (g_{\rm eff}^{(2)})^2}$, and $g_{\rm eff}^{(1)}$ and $g_{\rm eff}^{(2)}$ are given by equation (25) and the effective detunings all are set to zero. The time evolution of the coefficient c_{a110}, with the initial conditions $c_{a101}(t = 0) = 1$, $c_d(0) = 0$, and $c_{a110}(0) = 0$, reads

$$\begin{aligned} c_{a110} = {} & \frac{g_{\rm eff}^{(1)} g_{\rm eff}^{(2)}}{\bar{g}^2} \exp\left(-\frac{3\kappa}{2}t\right) \\ & \times \left\{-1 + \left[\cos(\lambda t) - \left(\frac{\kappa - 2\Gamma}{4\lambda}\right)\sin(\lambda t)\right] \right. \\ & \left. \times \exp\left(\frac{\kappa - 2\Gamma}{4}t\right)\right\}. \end{aligned} \tag{28}$$

Figure 10 demonstrates the population loss by either the spontaneous emission Γ, or by the cavity field decay κ.

In the absence of spontaneous emission Γ it is clear that the Fredkin gate is more sensitive to the cavity field decay rate κ (see equations (23) and (28). However, the fast iSWAP and the Fredkin gates (i.e. as effective three-level systems) have the same sensitivity to the spontaneous emission when no photonic decay is considered. Following the arguments in section 4, this gate shows great promise in QIP applications within recent cavity QED techniques.

5.4. Single qubit gates

For completeness, and recognising that we need single qubit rotations to make a universal set of gates, we turn briefly to an overview, based on reference [14], of how that can be achieved with the system we have. We start, in figure 11, with a lambda atom which has two transitions coupled to two cavity modes that make up a qubit, and we add a classical field to allow a return to the original atomic state $|a\rangle$. (This system is similar to the two-mode, two-classical field 'diamond' scheme of reference [46].) For our system, we will adiabatically eliminate levels $|b\rangle$ and $|c\rangle$ from the interaction under the conditions $\Delta_1, \Delta_2 \gg g_1^{ab}, g_2^{bc}, \Omega/2, \Delta_3$ (see appendix D) to find the effective detuning

$$\Delta_{\rm eff} = \Delta_3 + \frac{(g_1^{ab})^2}{\Delta_1}, \tag{29}$$

and the effective coupling

$$g_{\rm eff} = \frac{g_1^{ab} g_2^{bc} \Omega}{2\Delta_1 \Delta_2}. \tag{30}$$

We can then ensure a qubit rotation in the form

$$\hat{R}_x(g_{\rm eff}t) = \cos(g_{\rm eff}t/2)\hat{I} - i\,\sin(g_{\rm eff}t/2)\hat{\sigma}_x. \tag{31}$$

The Pauli Z gate can be easily realized by our qubits, too. Generally speaking, the atom-cavity interaction in the Jaynes–Cummings model shows that for an atom in the ground state $|g\rangle$ interacting with a single mode having n photons:

$$|g, n\rangle \mapsto \cos(g\sqrt{n}t)|g, n\rangle - i\,\sin(g\sqrt{n}t)|e, n-1\rangle.$$

This is the case when the frequencies of the atomic transitions and the mode are equally matched (i.e. the resonance case $\omega_{eg} = \omega$). In the case of very large detuning ($\Delta \gg g$), on the other hand, the system remains in its initial state and a phase shift can be produced as

$$|g, n\rangle \mapsto e^{i\Phi(n)}|g, n\rangle, \tag{32}$$

with $\Phi(n)$ can be expressed as [47]

$$\Phi(n) = \frac{\Delta}{2v}\int_0^L dz \left[\sqrt{1 + n\left(\frac{g(z)}{\Delta/2}\right)^2} - 1\right], \tag{33}$$

where v is the velocity of the atom passing through a cavity, L is the cavity length, and $g(z)$ is the coupling constant which in our case is independent of z. By setting $n = 0$ nothing happens, but with a cavity being initially in the number state $|1\rangle$ (i.e. there is $n = 1$ photon) a set of phase gates can be realised and the rotation operator $\hat{R}_z$ can be produced. In the case of two modes inside the cavity interacting with an atom in the ground state $|a\rangle$, such a case in the dual-mode qubits $|a\,10\rangle$ and $|a\,01\rangle$, the previous argument can be followed to introduce a phase shift. That is, we can set a large detuning between the atom and, say the first mode, and set a very high detuning between

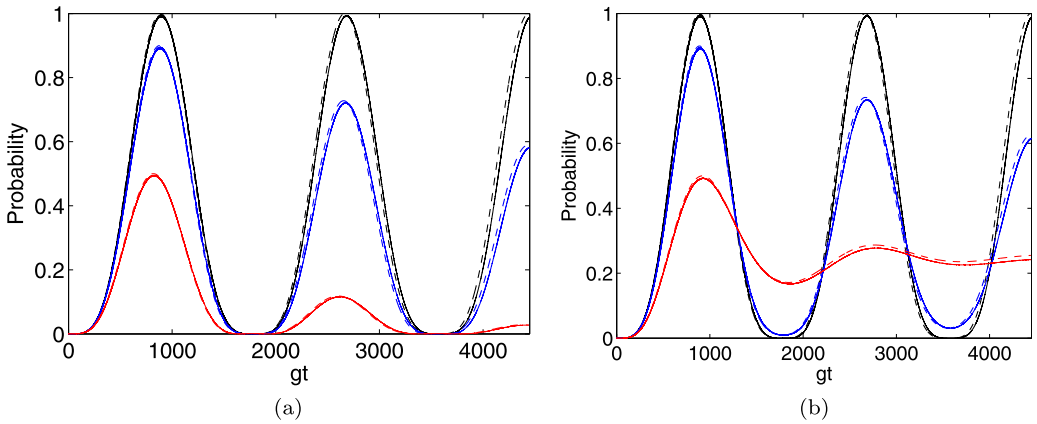

Figure 10. In (a) and (b) the probability of the qubit state $|a\ 110\rangle$ in the model (1001001) with non-vanishing photonic and atomic decays. Solid and dashed curves show the numerical and theoretical solutions, respectively. The coupling constants g_i $(i = 1, 2, 3, 5, 6)$ all are set to g, and the detunings $\Delta_{1,2,4,5} = \Delta$ with $\Delta = 20g$. The effective couplings of the truncated system $g_{\rm eff}^{(1)}$ and $g_{\rm eff}^{(2)}$ are given by equation (25), and the detunings Δ_3 and Δ_6 are defined by the resonance conditions in equation (26). The black, blue, and red lines respectively represent (at the interaction time $gt_{\rm int}$) the system probability $P \sim (100, 90, 50)\%P_0$ with a maximum probability $P_0 \sim 0.9950$. The three curves corresponding to the values of: (a) the photonic decay rates $\kappa \sim (0,\ 0.0174,\ 0.1186)\bar{g}/\sqrt{2}$ with $\Gamma \mapsto 0$, and (b) the atomic decay rates $\Gamma \sim (0,\ 0.0976,\ 0.764)\bar{g}/\sqrt{2}$ with $\kappa \mapsto 0$.

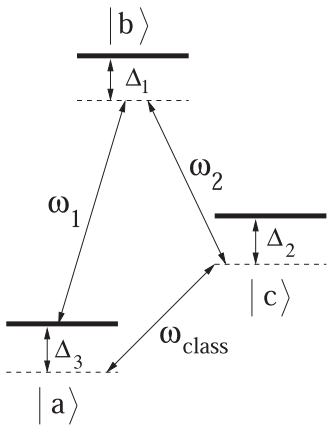

Figure 11. The model for a single-qubit Pauli-X gate. A three-level atom with Λ configuration of levels interacting with the optical cavity modes ω_1 and ω_2 on the transitions $|a\rangle \leftrightarrow |b\rangle$ and $|b\rangle \leftrightarrow |c\rangle$. The transition $|c\rangle \leftrightarrow |a\rangle$ is coupled by the classical field $\omega_{\rm class}$.

the atom and the second mode. In this case, if the excitation is in the first mode, one finds $|a\ 10\rangle \mapsto e^{ig^2t/\Delta}|a\ 10\rangle$; otherwise, $|a\ 01\rangle \mapsto |a\ 01\rangle$.

Different ways can be considered to add a global phase ζt to the gates already discussed in the previous sections. For instance, the single-qubit phase gate above can be employed for this purpose. That is, in the case of the previous iSWAP gate and after producing the transformations in section 3, an atom initially in the ground state $|a\rangle$ sent to the first two-mode cavity can introduce a phase to the logical state $|a\ 10\rangle$ when the atom is detuned from the first mode $\hat{n}_1$ of a qubit, and far detuned from the mode $\hat{n}_2$. Then, another atom in $|a\rangle$ interacting with the second two-mode cavity, where the atom is detuned from $\hat{n}_4$ and far detuned from $\hat{n}_3$, can add a phase to the logic $|a\ 01\rangle$.

6. Conclusion

In summary, our cavity QED systems realize two- and three-qubit gates. It is observed that a multiphoton resonance can be a useful technique for applications in quantum information processing as it involves a process conditional on the presence of various photons. Here we use the theory of multiphoton resonance with a multilevel multiphoton Jaynes–Cummings model. Information is stored in photonic qubits and we produce a set of practical one-qubit, two-qubit, and even three-qubit gates. This works because CQED in a strong-coupling regime offers a high non-linearity with low losses.

The gate interaction time follows from the different expressions for $g_{\rm eff}$ and depends on the system, i.e. iSWAP, fast-iSWAP, fast-Fredkin, etc. However, the general form is of order Δ^N/g^{N+1}, where there is a prefactor and N is an integer. However, the adiabatic elimination requires $\Delta \gg g$ and as seen in, for example, figure 5 it steadily improves as Δ/g increases. This does mean that the better the adiabatic condition, the slower the gate. However, a conditional measurement on the ancilla atom can improve the gate operation, without having infinite detuning.

The results of this paper allow us to consider, at these low levels of photonic excitation, whether a bigger practical issue is the spontaneous emission or the cavity decay. What we have found is that for all gates described in this manuscript, the loss of population due to the cavity field decay rate is more significant than the loss of poulation due to spontaneous emission. Table 2 shows the numerical values of atomic and photonic decays needed for reaching 90% and 50% of the maximum fidelity F_0 (where F_0 is the fidelity of these systems at resonance and in the absence of any decay). It is clear from this table that, firstly, the sensitivity to the atomic decay is almost the same in both the model (1001001) in

Table 2. A comparison between the damped iSWAP models (10 001) and (11 001), and the Fredkin gate model (1001 001). The detuning Δ is set to $15g$. The corresponding values of decay for 90% and 50% fidelity have been given above by Γ_i and κ_i with $i = 1, 2$, respectively.

Logic gate	The iSWAP gate (10 001)	(11 001)	The Fredkin gate (1001 001)
Interaction time	$5314.8\ /g$	$500.2\ /g$	$499.8/g$[2ex]
Atomic-decay	—	$\Gamma_1 \mapsto 0.42g$	$\Gamma_1 \mapsto 0.3g$
($\Gamma \times 10^{-3}$,$\kappa = 0$)	—	$\Gamma_2 \mapsto 3.25g$	$\Gamma_2 \mapsto 3.0g$[2ex]
Photonic-decay	$\kappa_1 \mapsto 0.01g$	$\kappa_1 \mapsto 0.12g$	$\kappa_1 \mapsto 0.075g$
($\kappa \times 10^{-3}$,$\Gamma = 0$)	$\kappa_2 \mapsto 0.07g$	$\kappa_2 \mapsto 0.80g$	$\kappa_2 \mapsto 0.500g$

the Fredkin gate and the model (11001) in the iSWAP gate. This is because these models have only one unblocked upper state. The model (10001) in the iSWAP gate is less sensitive to Γ decay since all upper states are blocked. Secondly, the model (10001) in the iSWAP gate is more sensitive to cavity decay (κ) since the interaction time in this gate is so long. The sensitivity to photonic decay is more in the model (1001001) in the Fredkin gate compared to the model (11001) in the iSWAP gate since it has more modes and more excitations.

Recently, the strong interaction between a multilevel atom with a multimode field (such as the interactions proposed in our scheme) has been of considerable interest in constructing experiments and is experimentally achievable with the current development in the resonator systems [48–50]. This promises that sufficiently strong interactions between a multilevel atom and a multimode field can be achievable [18], and therefore our scheme can be realized by present cavity QED technology. In addition, it is possible to create analogue systems with superconducting qubits (see, for example, references [20, 21]).

Acknowledgments

MMA would like to acknowledge support from University of Sussex. MSE thanks the Japanese Society for the Promotion of Science. BMG acknowledges the support of the Leverhulme Trust and thanks Michael Hartmann for helpful comments. BMG would like to especially thank Bruce W Shore for encouragement and comments on the development of this work.

Data availability statement

No new data were created or analysed in this study.

Appendix A. Adiabatic elimination

Generally, the time evolution of a quantum system is governed by the Schrödinger equation:

$$i\frac{\partial}{\partial t}\mathbf{c}(t) = \mathbf{H}\mathbf{c}(t). \tag{A1}$$

Applying a Laplace transform shows that

$$i(s\overline{\mathbf{c}}(s) - \mathbf{c}(0)) = \mathbf{H}\overline{\mathbf{c}}(s). \tag{A2}$$

An approximate solution in Laplace space, therefore, can be expressed as

$$\overline{\mathbf{c}}(s) = (s\mathbf{I} + i\mathbf{H})^{-1}\mathbf{c}(0). \tag{A3}$$

In Shore's method [23] we assume that the full Hamiltonian $\mathbf{H}$ is divided into $\mathbf{W}_0$ with states of interest, and states to be eliminated which are represented by the matrix $\mathbf{A}$ which is coupled to $\mathbf{W}_0$. In the cases which follow $\mathbf{W}_0$ is either a 2×2 matrix (appendices B1 and D) or a 3×3 matrix (appendices B2 and C). In either case $\mathbf{H}$ can be defined as $\mathbf{H} = \begin{bmatrix} \mathbf{W_0} & \mathbf{B} \\ \mathbf{B}^\dagger & \mathbf{A} \end{bmatrix}$.

Then, the inverse of the square matrix $(s\mathbf{I} + i\mathbf{H})$ reads

$$(s\mathbf{I} + i\mathbf{H})^{-1} = \begin{bmatrix} & -i\mathbf{X}\mathbf{B}(s + i\mathbf{A})^{-1} \\ -i(s + i\mathbf{A})^{-1}\mathbf{B}^\dagger\mathbf{X} & (s + i\mathbf{A})^{-1} - (s + i\mathbf{A})^{-1}\mathbf{B}^\dagger\mathbf{X}\mathbf{B}(s + i\mathbf{A})^{-1} \end{bmatrix}, \tag{A4}$$

where $\mathbf{X} = [s + i\mathbf{W}_0 + \mathbf{B}(s + i\mathbf{A})^{-1}\mathbf{B}^\dagger]^{-1}$.

Equation (A4) can be further simplified by introducing the approximation that the eigenvalues of $\mathbf{A}$ are much larger in magnitude than the eigenvalues of $\mathbf{W}_0$ [23]. One then finds that

$$(s\mathbf{I} + i\mathbf{H})^{-1} \sim \begin{bmatrix} [s + i(\mathbf{W}_0 - \mathbf{B}\mathbf{A}^{-1}\mathbf{B}^\dagger)]^{-1} & \mathcal{O}(1/A) \\ \mathcal{O}(1/A) & \mathcal{O}(1/A) \end{bmatrix}.$$

The subsystem containing only the states of interest can be, therefore, described by the effective Hamiltonian $\mathbf{H}_{\text{eff}} = \mathbf{W}_0 - \mathbf{B}\mathbf{A}^{-1}\mathbf{B}^\dagger$.

Appendix B. The iSWAP gate

B1. A two-level approximation

In this Appendix we derive key parameters g_{eff} and Δ_{eff} for the effective two-state version of the iSWAP gate. This is

to compare with the three-state version in appendix B2. For further details of the two-state version see reference [14]. In section 2, we have seen that in the interaction picture, and with $|a\ 1010\rangle$ to be the initial state, the Hamiltonian of the atom-field system is:

$$\hat{H}' = \begin{pmatrix} 0 & g_1^{ab} & 0 & 0 & 0 \\ g_1^{ab} & \Delta_1 & g_2^{bc} & 0 & 0 \\ 0 & g_2^{bc} & \Delta_2 & g_3^{cd} & 0 \\ 0 & 0 & g_3^{cd} & \Delta_3 & g_4^{da} \\ 0 & 0 & 0 & g_4^{da} & \Delta_4 \end{pmatrix}, \tag{B1}$$

where the system detunings Δ_i $(i = 1, 2, 3, 4)$ can be defined as

$$\begin{aligned} \Delta_1 &= (\omega_{ba} - \omega_1), \\ \Delta_2 &= (\omega_{ba} - \omega_1) - (\omega_{bc} - \omega_2), \\ \Delta_3 &= (\omega_{ba} - \omega_1) - (\omega_{bc} - \omega_2) + (\omega_{dc} - \omega_3), \\ \Delta_4 &= (\omega_{ba} - \omega_1) - (\omega_{bc} - \omega_2) + (\omega_{dc} - \omega_3) - (\omega_{da} - \omega_4). \end{aligned} \tag{B2}$$

By following Shore's method above, the basis states given by $|\Psi(t)\rangle$ in equation (5) can be divided into a couple of subsystems $\mathbb{P}|\Psi(t)\rangle$ and $\mathbb{Q}|\Psi(t)\rangle$, where $\mathbb{P}$ and $\mathbb{Q}$ are orthogonal projection operators and $\mathbb{P} + \mathbb{Q} = 1$. Assuming $\mathbb{P}$ consists of the states $|a10\rangle$ and $|a01\rangle$, one finds that the operators $H_0 = \mathbb{P}H\mathbb{P}$, $A = \mathbb{Q}H\mathbb{Q}$, and $B = \mathbb{P}H\mathbb{Q}$ can be expressed, in the matrix formalism, as

$$\begin{aligned} H_0 &= \begin{bmatrix} 0 & 0 \\ 0 & \Delta_4 \end{bmatrix}, \quad B = \begin{bmatrix} g_1^{ab} & 0 & 0 \\ 0 & 0 & g_4^{ad} \end{bmatrix}, \\ A &= \begin{bmatrix} \Delta_1 & g_2^{bc} & 0 \\ g_2^{bc} & \Delta_2 & g_3^{cd} \\ 0 & g_3^{cd} & \Delta_3 \end{bmatrix}. \end{aligned} \tag{B3}$$

An effective two-level Hamiltonian H_{eff} can be constructed by $H_{\text{eff}} = H_0 - BA^{-1}B^{\dagger}$. The effective coupling is found to be

$$\begin{aligned} g_{\text{eff}} &= -\frac{g_1^{ab} g_2^{bc} g_3^{cd} g_4^{da}}{\Delta_1\Delta_2\Delta_3 - \Delta_3(g_2^{bc})^2 - \Delta_1(g_3^{cd})^2}, \\ &\approx -\frac{g_1^{ab} g_2^{bc} g_3^{cd} g_4^{da}}{\Delta_1\Delta_2\Delta_3}, \end{aligned} \tag{B4}$$

and the effective detuning of the two-level system is

$$\begin{aligned} \Delta_{\text{eff}} &= \Delta_4 + \frac{(g_1^{ab})^2(\Delta_2\Delta_3 - (g_3^{cd})^2) - (g_4^{da})^2(\Delta_1\Delta_2 - (g_2^{bc})^2)}{\Delta_1\Delta_2\Delta_3 - \Delta_3(g_2^{bc})^2 - \Delta_1(g_3^{cd})^2}, \\ &\approx \Delta_4 + \frac{(g_1^{ab})^2}{\Delta_1} - \frac{(g_4^{da})^2}{\Delta_3}. \end{aligned} \tag{B5}$$

B2. . A three-level system

In the case of $\mathbb{Q} = |c, 0110\rangle\langle c, 0110| + |d, 0100\rangle\langle d, 0100|$, the operators H_0, B, and A can be given as

$$\begin{aligned} H_0 &= \begin{bmatrix} 0 & g_1^{ab} & 0 \\ g_1^{ab} & \Delta_1 & 0 \\ 0 & 0 & \Delta_4 \end{bmatrix}, \quad B = \begin{bmatrix} 0 & 0 \\ g_2^{bc} & 0 \\ 0 & g_4^{da} \end{bmatrix}, \\ A &= \begin{bmatrix} \Delta_2 & g_3^{cd} \\ g_3^{cd} & \Delta_3 \end{bmatrix}. \end{aligned} \tag{B6}$$

In the space $\{|a1010\rangle, |b0010\rangle, |a0101\rangle\}$, the effective Hamiltonian H_{eff} can be constructed as

$$H_{\text{eff}} = \begin{bmatrix} 0 & g_{(1)}^{\text{eff}} & 0 \\ g_{(1)}^{\text{eff}} & \Delta_1^{\text{eff}} & g_{(2)}^{\text{eff}} \\ 0 & g_{(2)}^{\text{eff}} & \Delta_2^{\text{eff}} \end{bmatrix}, \tag{B7}$$

and then the corresponding effective couplings and detunings can be expressed as

$$g_{\text{eff}}^{(1)} = g_1^{ab}, \quad g_{\text{eff}}^{(2)} = \frac{g_2^{bc} g_3^{cd} g_4^{da}}{(\Delta_2\Delta_3 - (g_3^{cd})^2)} \approx \frac{g_2^{bc} g_3^{cd} g_4^{da}}{\Delta_2\Delta_3}, \tag{B8}$$

and the effective detunings

$$\begin{aligned} \Delta_{\text{eff}}^{(1)} &= \Delta_1 - \frac{(g_2^{bc})^2\Delta_3}{(\Delta_2\Delta_3 - (g_3^{cd})^2)} \approx \Delta_1 - \frac{(g_2^{bc})^2}{\Delta_2}, \\ \Delta_{\text{eff}}^{(2)} &= \Delta_4 - \frac{(g_4^{da})^2\Delta_2}{(\Delta_2\Delta_3 - (g_3^{cd})^2)} \approx \Delta_4 - \frac{(g_4^{da})^2}{\Delta_3}. \end{aligned} \tag{B9}$$

Appendix C. A fast Fredkin gate

The Fredkin gate, as a three-qubit gate, can be realized in our scheme as mentioned in section 5. Considering figure 8, this system is governed by the Hamiltonian H

$$\begin{aligned} \hat{H} = \sum_i \omega_i \hat{\sigma}_{ii} + \sum_j \omega_j \hat{a}_j^{\dagger}\hat{a}_j + \Big[& g_1\ \hat{\sigma}_{ba}\ \hat{a}_1 + g_2\ \hat{\sigma}_{cb}\ \hat{a}_2^{\dagger} \\ & + g_3\ \hat{\sigma}_{dc}\ \hat{a}_3 + g_1\ \hat{\sigma}_{ed}\ \hat{a}_1^{\dagger} + g_5\ \hat{\sigma}_{fe}\ \hat{a}_5 + g_6\hat{\sigma}_{af}\ \hat{a}_6^{\dagger} + \text{h.c.}\Big], \end{aligned} \tag{C1}$$

where $(i = a, b, c, d, e, f)$ and $(j = 1, 2, 3, 5, 6)$. Beginning with the initial state of the atom-field system $|\Psi(0)\rangle = |a\ 10, 01, 10\rangle \equiv |a\ 101\rangle$, the time evolution of $|\Psi(0)\rangle$ can be a superposition

$$\begin{aligned} |\Psi(t)\rangle = & c_1(t)|a\ 10, 01, 10\rangle + c_2(t)|b\ 00, 01, 10\rangle \\ & + c_3(t)|c\ 00, 11, 10\rangle + c_4(t)|d\ 00, 10, 10\rangle \\ & + c_5(t)|e\ 10, 10, 10\rangle + c_6(t)|f\ 10, 10, 00\rangle \\ & + c_7(t)|a\ 10, 10, 01\rangle + c_8(t)|b\ 00, 10, 01\rangle \\ & + c_9(t)|c\ 00, 20, 01\rangle. \end{aligned} \tag{C2}$$

As shown above, the system does not terminate in the atomic state $|a\rangle$, and this system has the over-shot states $|b\ 00, 10, 01\rangle$ and $|c\ 00, 20, 01\rangle$. To avoid these states to be populated, we always assume the detunings Δ_1 and Δ_2 to be very large. The definitions of the detunings in equation (B2) can be easily employed to define the system detunings Δ_i (with $i = 1, 2, \ldots, 6$) in the Fredkin gate.

An effective three-level behaviour can be analysed by allowing the $\mathbb{P}$-space to include $|a, 101\rangle$, $|\mathrm{d}\rangle$, and $|a, 110\rangle$. The states $|b, 00, 01, 10\rangle, |c, 00, 11, 10\rangle$, $|e, 10, 10, 10\rangle, |f, 10, 10, 00\rangle, |b, 00, 10, 01\rangle$, and $|c, 00, 20, 01\rangle$ must be off-resonant so that they remain unpopulated. The required matrices for the effective Hamiltonian $H_{\rm eff} = H_0 - BA^{-1}B^{\dagger}$ can be expressed as

$$H_0 = \begin{bmatrix} 0 & 0 & 0 \\ 0 & \Delta_3 & 0 \\ 0 & 0 & \Delta_6 \end{bmatrix}, \quad B = \begin{bmatrix} g_1^{ab} & 0 & 0 & 0 & 0 & 0 \\ 0 & g_3^{cd} & g_1^{de} & 0 & 0 & 0 \\ 0 & 0 & 0 & g_6^{af} & g_1^{ab} & 0 \end{bmatrix},$$

$$A = \begin{bmatrix} \Delta_1 & g_2^{bc} & 0 & 0 & 0 & 0 \\ g_2^{bc} & \Delta_2 & 0 & 0 & 0 & 0 \\ 0 & 0 & \Delta_4 & g_5^{ef} & 0 & 0 \\ 0 & 0 & g_5^{ef} & \Delta_5 & 0 & 0 \\ 0 & 0 & 0 & 0 & \Delta_6 + \Delta_1 & g_2^{bc}\sqrt{2} \\ 0 & 0 & 0 & 0 & g_2^{bc}\sqrt{2} & \Delta_6 + \Delta_2 \end{bmatrix}. \tag{C3}$$

Within states $|10, 01, 10, a\rangle$, $|00, 10, 10, d\rangle$ and $|10, 10, 01, a\rangle$, the effective Hamiltonian $H_{\rm eff}$ can be given by equation (B7) where

$$g_1^{\rm eff} = \frac{g_1^{ab} g_2^{bc} g_3^{cd}}{\Delta_1 \Delta_2} \qquad g_2^{\rm eff} = \frac{g_1^{de} g_5^{ef} g_6^{fa}}{\Delta_4 \Delta_5},$$

and

$$\Delta_1^{\rm eff} \approx \Delta_3 + \frac{\left(g_1^{ab}\right)^2}{\Delta_1} - \frac{\left(g_3^{cd}\right)^2}{\Delta_2} - \frac{\left(g_1^{de}\right)^2}{\Delta_4},$$

$$\Delta_2^{\rm eff} \approx \Delta_6 - \frac{\left(g_6^{af}\right)^2}{\Delta_5}.$$

Appendix D. The not gate

The realisation of the single-qubit NOT gate is possible in our scheme. Considering the model in figure 11, we assume a de-excited three-level atom in the Λ configuration interacts with a dual-mode photonic qubit $|10\rangle$ or $|01\rangle$. The initial state, therefore, can be either the logic $|a\ 10\rangle$ or $|a\ 01\rangle$. Then, the atom interacts with a classical field on the transition $|c\rangle \mapsto |a\rangle$. The corresponding Hamiltonian describing all such interactions, i.e. the cavity-atom interaction plus the classical field-atom interaction, can be defined as

$$\hat{H} = \omega_a \hat{\sigma}_{aa} + \omega_b \hat{\sigma}_{bb} + \omega_c \hat{\sigma}_{cc} + \omega_1 \hat{a}_1^{\dagger}\hat{a}_1 + \omega_2 \hat{a}_2^{\dagger}\hat{a}_2 + \left[g_1^{ab}\hat{a}_1^{\dagger}\hat{\sigma}_{ab} + g_2^{bc}\hat{\sigma}_{bc}\hat{a}_2 + (\Omega/2)e^{i\omega_3 t}\hat{\sigma}_{ac} + \text{h.c.}\right]. \tag{D1}$$

Given the system in the initial state $|\Psi(0)\rangle = |a\ 10\rangle$, this state evolves into a superposition

$$|\Psi(t)\rangle = c_{c10}(t)|c\ 10\rangle + c_{a10}(t)|a\ 10\rangle + c_{b00}(t)|b\ 00\rangle + c_{c01}(t)|c\ 01\rangle + c_{a01}(t)|a\ 01\rangle. \tag{D2}$$

Then, by using the Schrödinger equation $\frac{\partial}{\partial t}|\Psi(t)\rangle = -i\hat{H}|\Psi(t)\rangle$ a set of amplitude equations, within the rotating wave approximation, can be obtained. To transform these amplitude equations to the frame rotating with the frequencies of the optical fields ω_1, ω_2, and $\omega_{\rm class}$, we introduce the transformation (note that the initial state $|a\ 10\rangle$ is set as a zero point energy)

$$\begin{aligned} c_{c10}(t) &= c'_{c10}(t)e^{-i(\omega_a+\omega_{\rm class})t}\, e^{-i\omega_1 t}; \\ c_{a10}(t) &= c'_{a10}(t)e^{-i\omega_a t}\, e^{-i\omega_1 t}; \\ c_{b00}(t) &= c'_{b00}(t)e^{-i(\omega_a+\omega_1)t}; \\ c_{c01}(t) &= c'_{c01}(t)e^{-i(\omega_a+\omega_1-\omega_2)t}\, e^{-i\omega_2}; \\ c_{a01}(t) &= c'_{a01}(t)e^{-i(\omega_a+\omega_1-\omega_2-\omega_{\rm class})t}\, e^{-i\omega_2 t}. \end{aligned} \tag{D3}$$

The RWA Hamiltonian, then, can be re-expressed as

$$H' = \begin{bmatrix} (\Delta_2 - \Delta_3) & \Omega/2 & 0 & 0 & 0 \\ \Omega/2 & 0 & g_1^{ab} & 0 & 0 \\ 0 & g_1^{ab} & \Delta_1 & g_2^{bc} & 0 \\ 0 & 0 & g_2^{bc} & \Delta_2 & \Omega/2 \\ 0 & 0 & 0 & \Omega/2 & \Delta_3 \end{bmatrix}, \tag{D4}$$

where $\hat{H}'$ acts in the basis $\{|c\ 10\rangle|a\ 10\rangle, |b\ 00\rangle, |c\ 01\rangle, |a\ 01\rangle\}$. Now the basis states other than $|a\ 10\rangle$ and $|a\ 01\rangle$ can be adiabatically eliminated by recalling Shore's method. That is, we allow large values for Δ_1, Δ_2. In other words, we assume the sates $|a\ 10\rangle$ and $|a\ 01\rangle$ to be spanned by the space $\mathbb{P}$ and the remaining states to be set in the space of $\mathbb{Q}$. The resultant operators, then, can be given in matrix form as

$$H_0 = \begin{bmatrix} 0 & 0 \\ 0 & \Delta_3 \end{bmatrix}; \quad B = \begin{bmatrix} \Omega/2 & g_1^{ab} & 0 \\ 0 & 0 & \Omega/2 \end{bmatrix};$$
$$A = \begin{bmatrix} (\Delta_2 - \Delta_3) & 0 & 0 \\ 0 & \Delta_1 & g_2^{bc} \\ 0 & g_2^{bc} & \Delta_2 \end{bmatrix}. \tag{D5}$$

The corresponding effective detuning with $\Delta_{1,2} \gg g_{1,2}$, $\Omega/2, \Delta_3$ is

$$\begin{aligned} \Delta_{\rm eff} &= \Delta_3 - \frac{(\Omega/2)^2\Delta_1}{(\Delta_1\Delta_2 - (g_2^{bc})^2)} + \frac{(\Omega/2)^2}{(\Delta_2 - \Delta_3)} \\ &\quad + \frac{(g_1^{ab})^2\Delta_1}{(\Delta_1\Delta_2 - (g_2^{bc})^2)} \\ &\approx \Delta_3 + \frac{(g_1^{ab})^2}{\Delta_2}, \end{aligned} \tag{D6}$$

and the effective coupling strength is

$$g_{\rm eff} = \frac{(\Omega/2)g_1^{ab}g_2^{bc}}{(\Delta_1\Delta_2 - (g_2^{bc})^2)} \approx \frac{\Omega\ g_1^{ab}g_2^{bc}}{2\Delta_1\Delta_2}. \tag{D7}$$

At the resonance condition, the time evolution of the initial state $|a\ 10\rangle$ or $|a\ 01\rangle$ can be given by equation (9), and with an appropriate interaction time $g_{\rm eff}t_{\rm int}$ and a global phase the Pauli X gate can be easily realized, and the exponential of the NOT gate is nothing but the rotation operator $\hat{R}_x(g_{\rm eff}t)$.

ORCID iDs

Moteb M Alqahtani https://orcid.org/0000-0003-1318-0656
Mark S Everitt https://orcid.org/0000-0003-2142-4438
Barry M Garraway https://orcid.org/0000-0003-2351-3768

References

[1] Lounis B and Moerner W E 2000 *Nature* **407** 491
[2] Santori C, Pelton M, Solomon G, Dale Y and Yamamoto Y 2001 *Phys. Rev. Lett.* **86** 1502
[3] Kuhn A, Hennrich M, Bondo T and Rempe G 1999 *App. Phys.* B **69** 373
[4] Keller M, Lange B, Hayasaka K, Lange W and Walther H 2004 *Nature* **431** 1075
[5] Cirac J I and Zoller P 1995 *Phys. Rev. Lett.* **74** 4091
[6] Kok P, Munro W J, Nemoto K, Ralph T C, Dowling J P and Milburn G J 2007 *Rev. Mod. Phys.* **79** 135
[7] Jonathan A J, Michele M and Rasmus H H 1998 *Nature* **393** 344–6
[8] Hanson R and Awschalom D D 2008 *Nature* **453** 1043
[9] Raimond J M, Brune M and Haroche S 2001 *Rev. Mod. Phys.* **73** 565
[10] Takahashi H, Kassa E, Christoforou C and Keller M 2020 *Phys. Rev. Lett.* **124** 013602
[11] Mabuchi H and Doherty A C 2002 *Science* **298** 1372
[12] van Enk S J, Kimble H J and Mabuchi H 2004 *Quantum Inf. Process.* **3** 75
[13] Walther H, Varcoe B T H, Englert B G and Becker T 2006 *Rep. Prog. Phys.* **69** 1325
[14] Everitt M S and Garraway B M 2014 *Phys. Rev.* A **90** 012335
[15] Anders J, Oi D K L, Kashefi E, Browne D E and Andersson E 2010 *Phys. Rev.* A **82** 020301
[16] Grangier P, Reymond G and Schlosser N 2000 *Fortschr. Phys.* **48** 859
[17] Kjaergaard M, Schwartz M E, Braumüller J, Krantz P, Wang J I-J, Gustavsson S and Oliver W D 2020 *Annu. Rev. Condens. Matter Phys.* **11** 369
[18] Forn-Díaz P, Lamata L, Rico E, Kono J and Solano E 2019 *Rev. Mod. Phys.* **91** 025005
[19] Kuhr S *et al* 2007 *Appl. Phys. Lett.* **90** 164101
[20] Feng W and Wang D-W 2020 *Phys. Rev.* A **101** 062312
[21] Haroche S, Brune M and Raimond J M 2020 *Nat. Phys.* **16** 243
[22] Blais A, Grimsmo A L, Girvin S M and Wallraff A 2021 *Rev. Mod. Phys.* **93** 025005
[23] Shore B W 1981 *Phys. Rev.* A **24** 1413
[24] Alqahtani M M 2018 *Quantum Inf. Process.* **17** 211
[25] Alqahtani M M 2020 *Quantum Inf. Process.* **19** 12
[26] Chuang I L and Yamamoto Y 1995 *Phys. Rev.* A **52** 3489
[27] Chuang I L and Yamamoto Y 1996 *Phys. Rev. Lett.* **76** 4281
[28] Jaynes E T and Cummings F W 1963 *Proc. IEEE* **51** 89
[29] Cook R J and Shore B W 1979 *Phys. Rev.* A **20** 539
[30] Schuch N and Siewert J 2003 *Phys. Rev.* A **67** 032301
[31] Tanamoto T, Liu Y-X, Hu X and Nori F 2009 *Phys. Rev. Lett.* **102** 100501
[32] Raussendorf R and Briegel H J 2001 *Phys. Rev. Lett.* **86** 5188
[33] Raussendorf R, Browne D E and Briegel H J 2003 *Phys. Rev.* A **68** 022312
[34] Lindblad G 1976 *Commun. Math. Phys.* **48** 119
[35] Carmichael H 1991 *An Open System Approach to Quantum Optics* (*Lecture Notes in Physics*)vol 18) (Berlin: Springer)
[36] Dalibard J, Castin Y and Mølmer K 1992 *Phys. Rev. Lett.* **68** 580
[37] Mølmer K, Castin Y and Dalibard J 1993 *J. Opt. Soc. Am.* B **10** 524
[38] Garraway B M and Knight P L 1994 *Phys. Rev.* A **50** 2548
[39] Knight P L and Garraway B M 1996 *Proc. 44th Scottish Universities Summer School in Physics* (Bristol: IOP Publishing) ch quantum superpositions in dissipative environments: decoherence and deconstruction pp 199–238
[40] Plenio M B and Knight P L 1998 *Rev. Mod. Phys.* **70** 101
[41] Spehner D and Orszag M 2002 *J. Math. Phys.* **43** 3511
[42] Dum R, Zoller P and Ritsch H 1992 *Phys. Rev.* A **45** 4879
[43] Fredkin E and Toffoli T 1982 *Int. J. Theor. Phys.* **21** 219
[44] Nielsen M A and Chuang I L 2000 *Quantum Computation and Quantum Information* (Cambridge: Cambridge University Press)
[45] Barnett S M 2009 *Quantum Information* (Oxford: Oxford University Press)
[46] Chimczak G, Bartkiewicz K, Ficek Z and Tanaś R 2018 *Sci. Rep.* **8** 14740
[47] Englert B-G *et al* 1998 *Fortschr. Phys.* **46** 897
[48] Kollár A J, Papageorge A T, Vaidya V D, Guo Y, Keeling J and Lev B L 2017 *Nat. Commun.* **8** 14386
[49] Hamsen C, Tolazzi K N, Wilk T and Rempe G 2018 *Nat. Phys.* **14** 885
[50] Sundaresan N M, Liu Y, Sadri D, Szöcs L J, Underwood D L, Malekakhlagh M, Türeci H E and Houck A A 2015 *Phys. Rev.* X **5** 021035